Range Extension Autonomous Driving for Electric Vehicles Based on Optimal Vehicle Velocity Trajectory Generation and Front–Rear Driving–Braking Force Distribution with Time Constraint

Yuta Ikezawa*a) Student Member, Hiroshi Fujimoto* Senior Member
Yoichi Hori* Fellow

Electric vehicles (EVs) have been intensively studied in the last decade due to their environment friendly characteristics. However, the miles–per–charge of EVs is shorter than that of internal combustion engine vehicles. To improve miles–per–charge, the authors' group has proposed Range Extension Control Systems (RECS) and Range Extension Autonomous Driving (READ) system. One problem with the conventional READ system is that the time constraint was not addressed for practical usage. In this paper, by considering time constraint, READ system which optimizes velocity trajectory and distribution ratio energy saving is proposed for autonomous driving vehicles. The effectiveness of the proposed method is verified by simulations and experiments.

Keywords: electric vehicle, driving and braking force distribution, range extension autonomous driving, slip ratio, motor loss, electromechanical brake

1. Introduction

Due to the increasing concerns on environmental and energy problems, electric vehicles (EVs) have been widely studied in the last decade. Compared with internal combustion engine vehicles (ICEVs), EVs have the following remarkable advantages [(1)].

(1) Torque generation of motors is faster than that of engines (several milliseconds vs. several hundred milliseconds).
(2) Motor torque enable to be estimated precisely from the current.
(3) Small but powerful motors can be installed in each wheel, and can be independently controlled.
(4) Not only driving, but also regenerative braking are available.

Although EVs have many advantages, they have one problem that the miles–per–charge is short. In order to solve this problem, many kinds of researches have been conducted, for example, wireless power transfer for moving electric vehicles, expanding high–efficiency regions of motors, and new types of power train [(2)~(4)]. On the other hand, the authors' research group has proposed Range Extension Control Systems (RECS) [(5)(6)], which do not need to change the vehicle structures. By utilizing the difference of front and rear motor efficiencies, RECS distributes total driving–braking force between front and rear wheels to extend miles–per–charge. For the distribution algorithm, several methods are available, for instance, one study proposed a searching algorithm to decide the distribution ratio for loss minimization [(5)], another one focused on finding the optimal solution analytically by modeling the consumption energy [(6)].

Most of the conventional researches on RECS were carried out on condition that the driver decides the vehicle velocity. However, along with the development of intelligent transport systems (ITS) [(7)] and autonomous driving technologies, vehicle velocity control has to be considered for energy efficiency improvement. If vehicle velocity can be controlled automatically, various energy management systems are possible by optimizing the vehicle velocity. For example, minimizing the consumption energy with time constraint is possible, and this is especially effective in saving remaining energy during commuting. A recent article considered the time constraint for the minimization of consumption energy of EVs [(8)]. Nevertheless, important factors such as load fluctuation, slip ratio and motor loss were not taken into account.

In this paper, by considering distribution ratio, load fluctuation, slip ratio, motor loss, and time constraint, a Range Extension Autonomous Driving (READ) system which minimizes the consumption energy is proposed for autonomous driving vehicles. One of the problems with the proposed method is that the copper loss is large when the vehicle decelerates to a very low speed. To solve this problem, a switching method between regenerative brake and electromechanical brake [(9)] is also proposed. The effectiveness of the proposed methods are verified by simulations and experiments.

2. Experimental Vehicle and Vehicle Model

2.1 Experimental Vehicle In this research, an original electric vehicle "FPEV–2 Kanon," manufactured by the authors' research group, is used. Fig. 1 shows the experimental vehicle. This vehicle has four outer–rotor type in–wheel motors. Therefore, driving–braking force distribution among all the wheels is possible. Fig. 2 shows efficiency maps of the front and rear in–wheel motors. RECS is possible by us-

a) Correspondence to: ikezawa14@hflab.k.u-tokyo.ac.jp
* The University of Tokyo, 5-1-5 Kashiwanoha, Kashiwa, Chiba, 277-8561 Japan

Fig. 1. FPEV2–Kanon.

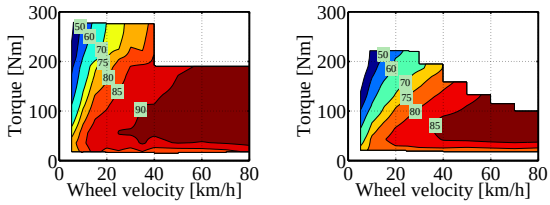

(a) Front motor. (b) Rear motor.

Fig. 2. Efficiency maps of front and rear motors.

Table 1. Vehicle specification.

Vehicle mass M	854 kg
Wheelbase l	1.72 m
Distance from center gravity to front and rear axle l_f,l_r	l_f:1.01 m l_r:0.702 m
Gravity height h_g	0.51 m
Front wheel inertia J_{ω_f}	1.24 kg·m^2
Rear wheel inertia J_{ω_r}	1.26 kg·m^2
Wheel radius r	0.302 m

Table 2. Specification of in–wheel motors.

	Front	Rear
Manufacturer	TOYO DENKI SEIZO K.K.	
Type	Direct Drive System	
Rated torque	110 Nm	137 Nm
Maximum torque	500 Nm	340 Nm
Rated power	6.00 kW	4.30 kW
Maximum power	20.0 kW	10.7 kW
Rated speed	382 rpm	300 rpm
Maximum speed	1110 rpm	1500 rpm

ing the different efficiencies to change the distribution ratio. Table 1 and Table 2 show the specification of the vehicle and the in–wheel motors, respectively.

2.2 Vehicle Model In this section, a four wheel driven vehicle is modeled. As only straight driving is considered, torques of right and left motors are equal. The equation of wheel rotation and vehicle dynamics are given as

$$J_{\omega_j}\dot{\omega}_j = T_j - rF_j, \quad (1)$$

$$M\dot{V} = F_{\mathrm{all}} - \mathrm{sgn}(V)F_{\mathrm{DR}}(V), \quad (2)$$

$$F_{\mathrm{all}} = 2\sum_{j=f,r} F_j, \quad (3)$$

where J_{ω_j} is the wheel inertia, ω_j is the wheel angular velocity, T_j is the motor torque, r is the wheel radius, F_j is the driving–braking force of each wheel, M is the vehicle mass, V is the vehicle velocity, F_{DR} is the driving resistance, F_{all} is the total driving–braking force, and sgn is a sign function. The subscript j represents f or r (f stands for front and r does for rear). The driving resistance F_{DR} is defined as

$$F_{\mathrm{DR}}(V) = \mu_0 Mg + b|V| + \frac{1}{2}\rho C_{\mathrm{d}} A V^2, \quad (4)$$

where μ_0 is the coefficient of rolling friction, b is the factor which is proportional to V, ρ is the air density, C_{d} is the drag coefficient, and A is the frontal projected area.

Next, the slip ratio λ_j is described as

$$\lambda_j = \frac{V_{\omega_j} - V}{\max(V_{\omega_j}, V, \epsilon)}, \quad (5)$$

where $V_{\omega_j} = r\omega_j$ is the wheel speed and ϵ is a small constant to avoid zero division. It is known the slip ratio λ is related with the coefficient of friction μ [10]. In region $|\lambda| << 1$, μ is nearly proportional to λ. Let the driving stiffness D_{s}' be the slope of the curve, driving force of each wheel is given as

$$F_j = \mu_j N_j \approx D_{\mathrm{s}}' N_j \lambda_j, \quad (6)$$

where N_j is the normal force of each wheel. During driving at V and F_{all}, N_f and N_r are calculated as

$$N_f(V, F_{\mathrm{all}}) = \frac{1}{2}\left[\frac{l_r}{l}Mg - \frac{h_{\mathrm{g}}}{l}\{F_{\mathrm{all}} - \mathrm{sgn}(V)F_{\mathrm{DR}}(V)\}\right], \quad (7)$$

$$N_r(V, F_{\mathrm{all}}) = \frac{1}{2}\left[\frac{l_f}{l}Mg + \frac{h_{\mathrm{g}}}{l}\{F_{\mathrm{all}} - \mathrm{sgn}(V)F_{\mathrm{DR}}(V)\}\right], \quad (8)$$

where l_f and l_r are the distance from center gravity to front and rear axle, l is the wheelbase, and h_{g} is the gravity height.

During straight driving, required driving–braking force can be distributed to each wheel. Since the motors of the EVs assumed in this research can be independently controlled, a degree of freedom of the driving–braking force distribution exists. By introducing front and rear driving–braking force distribution ratio k, driving–braking forces can be formulated based on F_{all} using the distribution ratio k, as follows:

$$F_j = \frac{1}{2}\gamma_j(k)F_{\mathrm{all}}, \quad (9)$$

$$\gamma_j(k) = \begin{cases} 1-k & (j=f) \\ k & (j=r) \end{cases}. \quad (10)$$

Distribution ratio k varies between 0 and 1. $k = 0$ means the vehicle is a front driven system, and $k = 1$ means rear driven only.

2.3 Inverter Input Power Model Neglecting the mechanical loss of the motor and inverter loss, inverter input power P_{in} is described as

$$P_{\mathrm{in}} = P_{\mathrm{out}} + P_{\mathrm{c}} + P_{\mathrm{i}}, \quad (11)$$

where P_{out} is the sum of mechanical output of each motor, P_{c} is the sum of copper loss of each motor, and P_{i} is the sum of iron loss of each motor [6].

In the modeling of mechanical loss P_{out}, let us suppose that the torque by the wheel inertia is small enough, and λ_j is small enough. Then, from Eq. (1), (5), (6), and (9), P_{out} is calculated as

$$P_{\mathrm{out}} = 2\sum_{j=f,r}\omega_j T_j$$

$$\simeq VF_{\mathrm{all}}\sum_{j=f,r}\left(1 + \frac{\gamma_j(k)F_{\mathrm{all}}}{2D_{\mathrm{s}}' N_j(V, F_{\mathrm{all}})}\right)\gamma_j(k). \quad (12)$$

In the modeling of the copper loss P_{c}, iron loss resistance is neglected for simplicity. Suppose that the magnet torque is much larger than the reluctance torque and that the q–axis current is much greater than the d–axis current. Then, the

sum of the copper loss P_c is given as

$$P_c = 2\sum_{j=f,r} R_j {i_{qj}}^2 \simeq \frac{r^2}{2}{F_{all}}^2 \sum_{j=f,r} \frac{R_j}{{K_{tj}}^2}{\gamma_j}^2(k) \cdots\cdots (13)$$

where R_j is the armature winding resistance of the motor, i_{qj} is the q–axis current, and K_{tj} is the torque coefficient of the motor. The sum of the iron loss P_i is expressed as

$$\begin{aligned} P_i &= 2\sum_{j=f,r} \frac{{v_{odj}}^2 + {v_{oqj}}^2}{R_{cj}} \\ &= 2\sum_{j=f,r} \frac{{\omega_{ej}}^2}{R_{cj}} \left\{ \left(L_{dj} i_{odj} + \Psi_j\right)^2 + \left(L_{qj} i_{oqj}\right)^2 \right\} \\ &\simeq 2\frac{V^2}{r^2} \sum_{j=f,r} \frac{{P_{nj}}^2}{R_{cj}} \left\{ \left(\frac{r L_{qj} \gamma_j(k) F_{all}}{2K_{tj}} \right)^2 + {\Psi_j}^2 \right\}, \cdots (14) \end{aligned}$$

where v_{odj} and v_{oqj} are d and q–axis induced voltage, R_{cj} is the equivalent iron loss resistance, ω_{ej} is the electrical angular velocity of each motor, L_{dj} is d–axis inductance, L_{qj} is q–axis inductance, i_{odj} and i_{oqj} are the difference between d and q–axis current and d and q–axis components of iron loss current respectively, P_{nj} is the number of pole pairs, and Ψ_j is the interlinkage magnetic flux. Equivalent iron loss resistance R_{cj} is described as

$$\frac{1}{R_{cj}(\omega_{ej})} = \frac{1}{R_{c0j}} + \frac{1}{R_{c1j}'|\omega_{ej}|}. \cdots\cdots\cdots\cdots\cdots\cdots (15)$$

In Eq. (15), the first and second terms of right hand side respectively mean eddy current loss and hysteresis loss.

3. Optimization of Velocity Trajectory and Driving–Braking Force Distribution Ratio

In this paper, the case that vehicle velocity which changes from $V_0(t_0)$ to $V_f(t_f)$ with a fixed travel distance is considered. This method optimizes the vehicle velocity trajectory and front–rear driving–braking force distribution which minimize consumption energy between t_0 and t_f. Therefore, the objective function and constraint conditions are expressed as

$$\begin{aligned} \text{min.} \quad & W_{in} = \int_{t_0}^{t_f} P_{in}(\boldsymbol{x}(t), \boldsymbol{u}(t))dt, \cdots\cdots\cdots\cdots (16) \\ \text{s.t.} \quad & \dot{\boldsymbol{x}} = \boldsymbol{f}(\boldsymbol{x}(t), \boldsymbol{u}(t)) \\ & = \begin{bmatrix} \frac{1}{M}(F_{all} - \mathrm{sgn}(V)F_{DR}(V)) \\ V(t) \end{bmatrix}, \cdots\cdots (17) \\ & \chi(\boldsymbol{x}(t_0)) = \boldsymbol{x}(t_0) - \boldsymbol{x_0} = \begin{bmatrix} V(t_0) - V_0 \\ X(t_0) - X_0 \end{bmatrix} = \boldsymbol{0}, \quad \cdots (18) \\ & \psi(\boldsymbol{x}(t_f)) = \boldsymbol{x}(t_f) - \boldsymbol{x_f} = \begin{bmatrix} V(t_f) - V_f \\ X(t_f) - X_f \end{bmatrix} = \boldsymbol{0}, \cdots\cdots (19) \end{aligned}$$

where W_{in} is the consumption energy, $\boldsymbol{x}$ is the state variable, $\boldsymbol{u}$ is the control variable, $\boldsymbol{x_0}$ is the initial condition, and $\boldsymbol{x_f}$ is the terminal condition. They are defined as

$$\boldsymbol{x}(t) = \begin{bmatrix} V(t) \\ X(t) \end{bmatrix}, \boldsymbol{u}(t) = \begin{bmatrix} F_{all}(t) \\ k(t) \end{bmatrix}. \cdots\cdots\cdots\cdots\cdots\cdots (20)$$

Vehicle velocity trajectory and driving–braking distribution ratio which minimize consumption energy can be calculated by solving this optimal control problem. Since $P_{in}(k)$ is a quadratic function of k, optimal distribution ratio k_{opt} which minimizes P_{in} satisfies $\partial P_{in}/\partial k|_{k=k_{opt}} = 0$. Therefore, k_{opt} is derived as a function of V and F_{all} as

$$k_{opt}(V, F_{all}) = \frac{\frac{V}{D_s' N_f(V,F_{all})} + \frac{r^2 R_f}{{K_{tf}}^2} + \frac{V^2}{R_{cf}(\omega_{ef})}\left(\frac{L_{qf}}{\Psi_f}\right)^2}{\frac{V}{D_s'}\sum_{j=f,r}\frac{1}{N_j(V,F_{all})} + r^2\sum_{j=f,r}\frac{R_j}{{K_{tj}}^2} + V^2\sum_{j=f,r}\frac{1}{R_{cj}(\omega_{ej})}\left(\frac{L_{qj}}{\Psi_j}\right)^2}. (21)$$

By applying k_{opt} at all times, this problem becomes one–dimensional search. In this paper, steepest descent method is used to calculate vehicle velocity trajectory.

Table 3. Acceleration time.

V_f [km/h]	Acceleration time [s]		
	Conventional	Proposed 1	Proposed 2
30	6.570	6.570	9.100
60	13.14	13.14	17.50

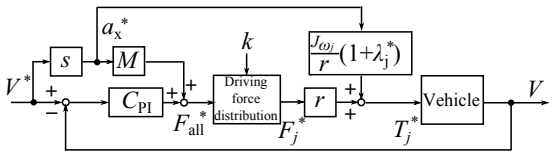

Fig. 3. Vehicle speed control system.

4. Optimal Vehicle Velocity Trajectory

4.1 Simulation In this section, to demonstrate the effectiveness of the proposed method, simulation is conducted under following 2 conditions.

Condition 1: The initial condition is determined as $V_0 = 0$ km/h, $t_0 = 0$ s, terminal condition is determined as $V_f = 30$ km/h, and travel distance $X_f - X_0 = 27.38$ m.

Condition 2: The initial condition is determined as $V_0 = 0$ km/h, $t_0 = 0$ s, terminal condition is determined as $V_f = 60$ km/h, and travel distance $X_f - X_0 = 109.5$ m.

In this paper, following 3 cases are considered for each case. Acceleration time of each case is decided as Table 3.

Conventional: The vehicle changes velocity from $V_0(t_0)$ to $V_f(t_f)$ at a constant acceleration under the condition that $k = 0.5$. Therefore the V and t_f are given as

$$V = V_0 + \frac{{V_f}^2 - {V_0}^2}{2(X_f - X_0)}(t - t_0), \cdots\cdots\cdots\cdots\cdots\cdots (22)$$

$$t_f = \frac{2(X_f - X_0)}{(V_f + V_0)} + t_0. \cdots\cdots\cdots\cdots\cdots\cdots\cdots\cdots (23)$$

Proposed 1: Optimize the vehicle velocity trajectory with time constraint to minimize consumption energy. The vehicle changes velocity from $V_0(t_0)$ to $V_f(t_f)$ under the condition that $k = k_{opt}$. Terminal time t_f is equal to that of conventional method.

Proposed 2: Optimize the vehicle velocity trajectory without considering time constraint to minimize consumption energy. The vehicle changes velocity from $V_0(t_0)$ to $V_f(t_{fopt})$ under the condition that $k = k_{opt}$.

This research was carried out on the assumption that the vehicle velocity can be controlled automatically. Fig. 3 shows vehicle velocity control system to control vehicle velocity automatically. The input is vehicle velocity reference V^*, and these controllers generate total driving–braking force reference ${F_{all}}^*$. And then, ${F_{all}}^*$is distributed to the front and rear

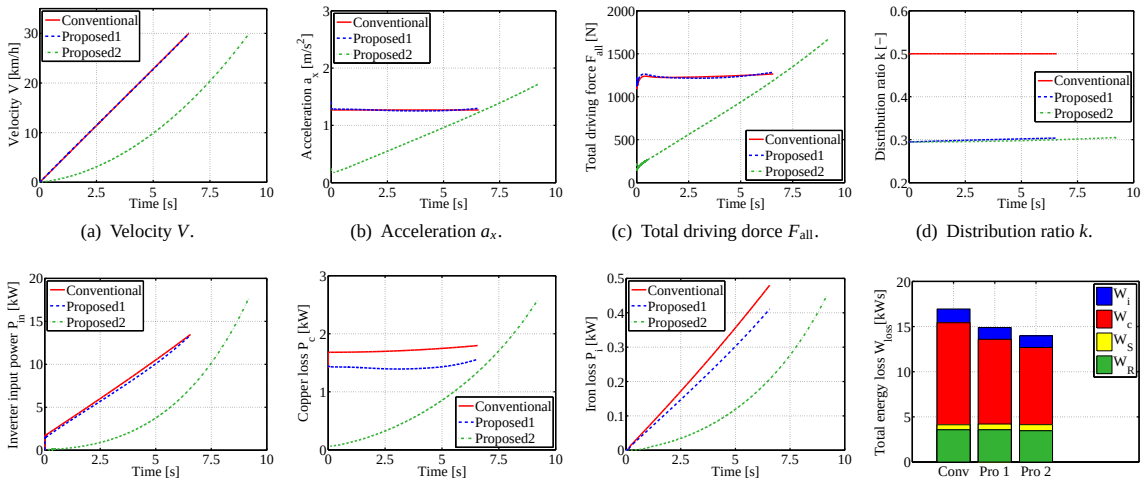

(a) Velocity V. (b) Acceleration a_x. (c) Total driving dorce F_{all}. (d) Distribution ratio k.

(e) Inverter input power P_{in}. (f) Copper loss P_{c}. (g) Iron loss P_{i}. (h) Total energy loss W_{loss}.

Fig. 4. Simulation results 1 (condition 1: V_f = 30 km/h, acceleration).

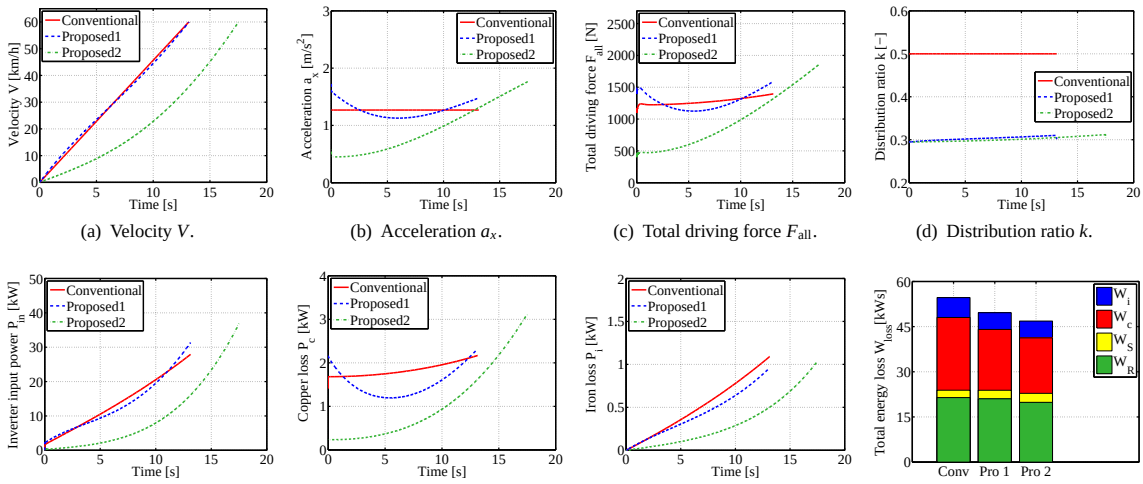

(a) Velocity V. (b) Acceleration a_x. (c) Total driving force F_{all}. (d) Distribution ratio k.

(e) Inverter input power P_{in}. (f) Copper loss P_{c}. (g) Iron loss P_{i}. (h) Total energy loss W_{loss}.

Fig. 5. Simulation results 2 (condition 2: V_f = 60 km/h, acceleration).

driving–braking force reference ${F_j}^*$. Considering slip ratio, front and rear torque reference ${T_j}^*$ is given as

$$ {T_j}^* = r{F_j}^* + \frac{J_{\omega_j}{a_x}^*}{r}(1+{\lambda_j}^*), \cdots\cdots\cdots\cdots\cdots\cdots (24) $$

where the second term of right hand side means compensation of inertia of the wheels. In this research, ${\lambda_j}^*$ is 0.05, 0, -0.05 during acceleration, cruising and deceleration.

Vehicle velocity controller C_{PI} is a PI controller, and it is designed by the pole placement method. The plant of vehicle velocity controller is expressed as

$$ \frac{V}{F_{\mathrm{all}}} = \frac{1}{Ms}. \cdots\cdots\cdots\cdots\cdots\cdots\cdots\cdots\cdots\cdots\cdots\cdots (25) $$

In the simulations and experiments, the poles of vehicle velocity controller is set to -5 rad/s.

Fig. 4 and Fig. 5 show simulation results. To analyze the simulation results, P_{out} is separated into the power stored as kinetic energyof vehicle mass P_{M}, the sum of the power stored as rotational energy of each wheel P_{J}, the loss caused by the driving resistance P_{R}, and the sum of the loss caused by slip of each wheel P_{S}. The integrated values of these values are described as

$$ W_X = \int_{t_0}^{t_{\mathrm{f}}} P_X(\boldsymbol{x}(t), \boldsymbol{u}(t))dt, \cdots\cdots\cdots\cdots\cdots\cdots\cdots (26) $$

where the subscript X represents “out”, “M”, “J”, “R”, “S”, “c”, and “i”. W_{M} and W_{J} can be recovered during decelerating, and they are equal in all cases if $V_0 = V_{\mathrm{f}}$. To evaluate the real loss, the total energy loss W_{loss} and the energy which can be recovered during decelerating W_{kinetic} are defined as

$$ W_{\mathrm{loss}} = W_{\mathrm{in}} - W_{\mathrm{M}} - W_{\mathrm{J}}, \cdots\cdots\cdots\cdots\cdots\cdots\cdots (27) $$

$$ W_{\mathrm{kinetic}} = W_{\mathrm{in}} - W_{\mathrm{loss}} = W_{\mathrm{M}} + W_{\mathrm{J}}. \cdots\cdots\cdots\cdots\cdots (28) $$

W_{kinetic} is 31.9 kWs in the condition 1, W_{kinetic} is 128 kWs in the condition 2.

Unlike the condition 1, acceleration of the proposed method 1 is larger than that of conventional method at $t < 2.5$ s and $t > 10$ s in the condition 2. As V becomes higher, percentage of copper loss to inverter input power becomes smaller. Generation of large acceleration at $t < 2.5$ s reduces required driving force at other speed region. Generation of large acceleration at $t > 10$ s shortens driving time at high speed, and reduce energy of iron loss and the loss by driving resistance.

Fig. 4(c) and Fig. 5(c) show that proposed method 2 generates smaller driving force at low speed than conventional

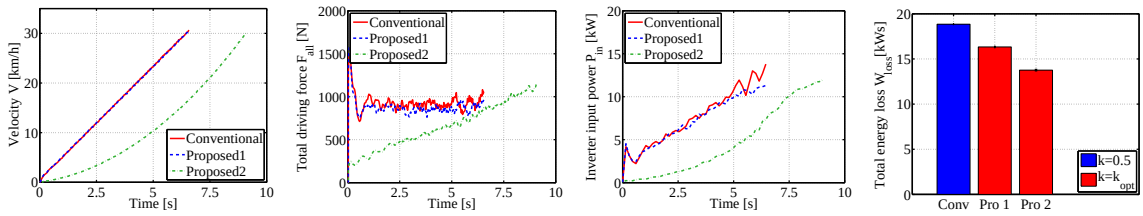

(a) Velocity V. (b) Total driving force F_{all}. (c) Inverter input power P_{in}. (d) Total energy loss W_{loss}.

Fig. 6. Experimental results 1 (condition 1: $V_{\mathrm{f}} = 30$ km/h, acceleration).

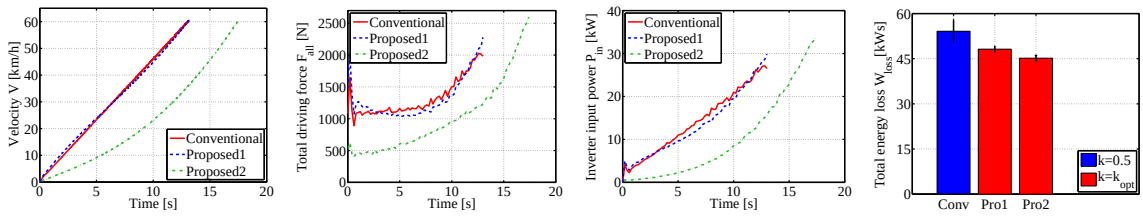

(a) Velocity V. (b) Total driving force F_{all}. (c) Inverter input power P_{in}. (d) Total energy loss W_{loss}.

Fig. 7. Experimental results 2 (condition 2: $V_{\mathrm{f}} = 60$ km/h, acceleration).

method. Therefore copper loss at low speed becomes smaller than conventional method as shown in Fig. 4(f) and Fig. 5(f). Larger driving force than conventional method at high speed shortens time driving with large iron loss as shown in Fig. 4(g) and Fig. 5(g). Therefore energy of iron loss becomes smaller than conventional method.

According to Fig. 2, efficiency of the front motor is better than that of the rear motor at all region. Therefore distribution ratio is nearly equal 0.3 at all time as shown in Fig. 4(d) and Fig. 5(d).

Compared with conventional method , proposed method 2 reduces 0.110 kWs of W_{R}, 2.75 kWs of W_{c} and 0.228 kWs of W_{i} in the condition 1, does 1.57 kWs of W_{R}, 5.75 kWs of W_{c} and 1.01 kWs of W_{i} in the condition 2. As V_{f} becomes higher, percentage of cutback of W_{c} to total cutback becomes lower. As a result, compared with conventional method, proposed method 1 and 2 respectively reduces about 12.2 % and 17.5 % total energy loss in the condition 1, does about 9.2 % and 14 % total energy loss in the condition 2.

4.2 Experiment Experiments were conducted 6 times under respective conditions, using the same conditions as simulations. In the experiments, we assumed that the velocity V is the average of all the wheel velocities. Inverter input power P_{in} was calculated as

$$P_{\mathrm{in}} = V_{\mathrm{dc}} \sum_{j=f,r} I_{\mathrm{dc}j}, \cdots\cdots\cdots\cdots\cdots\cdots\cdots\cdots\cdots (29)$$

where V_{dc} is the measured input voltage of inverter and $I_{\mathrm{dc}j}$ is the measured input current of front and rear inverter. P_{in} includes inverter loss.

Fig. 6 and Fig. 7 show experimental results. Fig. 7(b) shows that total driving–braking force became larger than that of simulation at high speed especially. It means that driving resistance includes modeling error. From Fig. 6(d) and Fig. 7(d) the results of total energy loss show the same tendency as simulation results. Compared with conventional method, proposed method 1 and 2 reduced about 13.4 % and 26.9 % total energy loss in the condition 1, did about 11.0 % and 16.5 % total energy loss in the condition 2.

5. Switching to Electromechanical Brake

5.1 Problem Formulation In this paper, a case that a vehicle which has velocity $V_0(t_0)$ starts to decelerate and stop at t_{f} with fixed travel distance is considered. Optimal velocity trajectory with time constraint has a problem that the copper loss is large when the vehicle decelerates to a very low speed. To avoid this problem, a case that a vehicle switches regenerative brake to electromechanical brake at velocity V_{s} is considered. Consumption energy after switching to electromechanical brake is neglected because it is small enough. Therefore the evaluation function is expressed as Eq. (30), and constraint conditions expressed as Eq. (31) are added.

$$\text{min.} \quad W_{\mathrm{in}} = \int_{t_0}^{t_{\mathrm{s}}} P_{\mathrm{in}}(\boldsymbol{x}(t), \boldsymbol{u}(t))dt, \cdots\cdots\cdots\cdots\cdots (30)$$

$$\text{s.t.} \quad \psi(\boldsymbol{x}(t_{\mathrm{s}})) = \boldsymbol{x}(t_{\mathrm{s}}) - \boldsymbol{x}_{\mathbf{s}} = \begin{bmatrix} V(t_{\mathrm{s}}) - V_{\mathrm{s}} \\ X(t_{\mathrm{s}}) - X_{\mathrm{f}} + \frac{{V_{\mathrm{s}}}^2 - {V_{\mathrm{f}}}^2}{2a_x} \end{bmatrix} = \mathbf{0}, (31)$$

where t_{s} is time to switch to electromechanical brake, a_x is deceleration after switching to electromechanical brake.

5.2 Simulation In this section, to demonstrate the effectiveness of proposed method, simulation is conducted. The initial condition is determined to $V_0 = 30$ km/h, $t_0 = 0$ s, terminal condition is determined to $V_{\mathrm{f}} = 0$ km/h, $t_{\mathrm{f}} = 6$ s, and travel distance $X_{\mathrm{f}} - X_0 = 27.38$ m. Method of using only regenerative brake ($V_{\mathrm{s}} = 0$ km/h) is treated as conventional method, method of switching regenerative brake to electromechanical brake at optimal velocity V_{sopt} is treated as proposed method. Deceleration a_x after switching to electromechanical brake is set to -2.5 m/s^2. In this paper, golden section method is used to detect V_{sopt}.

Fig. 8 shows simulation results. Fig. 8(a) and Fig. 8(b) show that proposed method generates large deceleration at low speed because it does not need to consider copper loss after switching to electromechanical brake. Fig. 8(c) shows that proposed method does not need to consume energy to decelerate. As a result, proposed method ($V_{\mathrm{s}} = V_{\mathrm{sopt}} = 5.5$ km/h) improved about 5.7 % regenerative energy compared

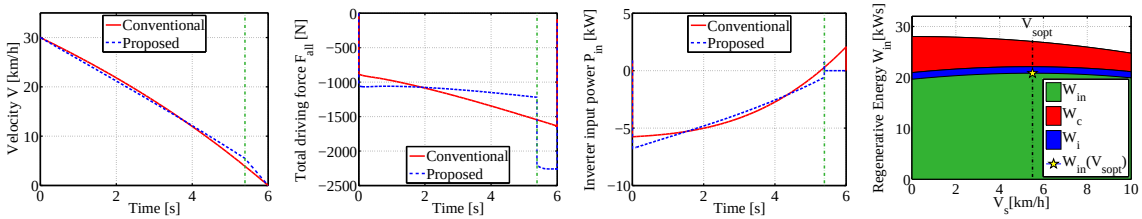

(a) Velocity V. (b) Total driving force F_{all}. (c) Inverter input power P_{in}. (d) Regenerative energy W_{in}.

Fig. 8. Simulation results 3 (switching to electromechanical brake).

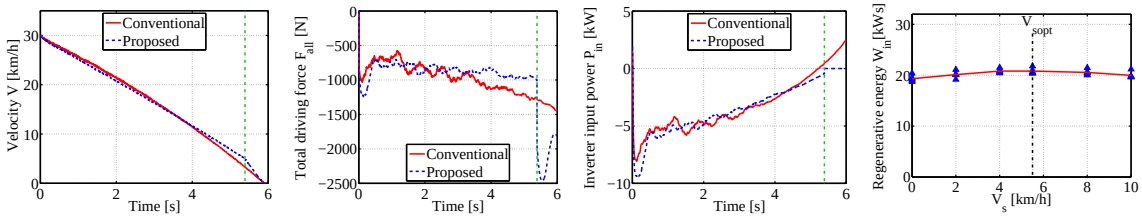

(a) Velocity V. (b) Total driving force F_{all}. (c) Inverter input power P_{in}. (d) Regenerative energy W_{in}.

Fig. 9. Experimental results 3 (switching to electromechanical brake).

with conventional method.

Fig. 8(d) indicates that W_{in} is a convex function of V_{s}. As V_{s} becomes lower, copper loss at low speed becomes larger because required total braking force at low speed becomes larger. As V_{s} becomes higher, W_{out} becomes smaller because kinetic energy lost through electromechanical brake becomes larger. Therefore, there is V_{sopt} which minimizes W_{in}.

5.3 Experiment Experiments were conducted 7 times under respective V_{s}, using the same conditions as the simulations. In this paper, regenerative brake was substituted for electromechanical brake, and consumption energy after switching to electromechanical brake was neglected. Fig. 9 shows the experimental results. Fig. 9(b) shows that the total driving force at 0 s became larger than that of simulation. It was caused by large jerk at that time. Therefore inverter input power at that time became larger than that of simulation. From Fig. 9(d), the results of regenerative energy show the same tendency as simulation results. Proposed method improved about 7.7 % regenerative energy compared with conventional method.

6. Conclusion

In this paper, an optimization method of vehicle velocity trajectory and driving–braking force distribution ratio with time constraint is proposed as READ. The effectiveness of the proposed method is verified by simulations and experiments. In the experimental results, proposed method reduced at most 26.9 % total energy loss compared with conventional method. Method of optimizing the timing of switching to electromechanical brake, vehicle velocity trajectory, and distribution ratio improved 7.7% regenerative energy.

Proposed method can apply to only straight driving. Therefore the future work is to introduce the velocity trajectory which minimizes consumption energy assuming the course which includes straight driving and cornering.

Acknowledgment

This research was partly supported by Industrial Technology Research Grant Program from New Energy and Industrial Technology Development Organization (NEDO) of Japan (number 05A48701d), and by the Ministry of Education, Culture, Sports, Science and Technology grant (number 22246057 and 26249061). In addition, we would like to thank National Traffic Safety and Environment Laboratory and Ono Sokki Co., Ltd. for offering the test course and the GPS speedometer.

References

(1) Y. Hori: “Future vehicle driven by electricity and control – research on four–wheel–motored “UOT Electric March II,”” IEEE Trans. on Industrial Electronics, Vol. 51, No. 5, pp. 954–962 (2004).

(2) J. Shin, S. Shin, Y. Kim, S. Ahn, S. Lee,G. Jung, S. J. Jeon, and D. H. Cho: “Design and Implementation of Shaped Magnetic–Resonance–Based Wireless Power Transfer System for Roadway–Powered Moving Electric Vehicles,” IEEE Trans. on Industrial Electronics, Vol. 61, No. 3, pp. 1179–1192 (2014).

(3) H. Hijikata, T. Shigeta, N. Kariya, K. Akatsu, and T. Kato: “A Study of Dual Winding Method for Compound Magnetomotive Force Motor,” IEEJ Trans. on Industry Applications, Vol. 133, No. 10, pp. 986–994 (2010) (in Japanese).

(4) M. Takeda, N. Motoi, G. Guidi, Y. Tsuruta, and A. Kawamura: “Driving Range Extension by Series Chopper Power Train of EV with Optimized dc Voltage Profile,” Proceedings of the 38th Annual Conference of the IEEE Industrial Electronics Society, pp. 2918–2923 (2012).

(5) H. Fujimoto, S. Egami, J. Saito, and K. Handa: “Range Extension Control System for Electric Vehicle Based on Searching Algorithm of Optimal Front and Rear Driving Force Distribution,” in Proc. 38th Annual Conference of the IEEE Industrial Electronics Society, pp. 4244–4249 (2012).

(6) S. Harada and H. Fujimoto: “Range Extension Control System Based on Optimization of Acceleration–Deceleration Trajectory and Front and Rear Driving–Braking Force Distribution,” Multi–symposium on Control Systems 2014,6F1–4 (2014) (in Japanese).

(7) J. Zhang, F. Y. Wang, K. Wang, W. H. Lin, X. Xu, and C. Chen: “Data–Driven Intelligent Transportation Systems:A Survey,” IEEE Trans. on Intelligent Transportation Systems, Vol. 12, No. 4, pp.1624–1639 (2011).

(8) T.Wang and C. G. Cassandras: “Optimal Motion Control for Energy–aware Electric Vehicles,” 2013 IEEE International Conference on Control Applications, pp. 388–393 (2013).

(9) T. Yamasaki, M. Eguchi, and Y. Makino: “Development of Electromechanical Brake,” NTN TECHNICAL REVIEW, No. 75, pp. 53–61 (2007).

(10) H. B. Pacejka and E. Bakker: “The Magic Formula Tyre Model,” Vehicle System Dynamics: International Journal of Vehicle Mechanics and Mobility, Vol. 21, No. 1, pp. 1–18 (1992).